Identification of Eu oxidation states in a doped $Sr_5(PO_4)_3F$ phosphor by TOF-SIMS imaging

H. C. Swart,[1,3*] I. M. Nagpure,[1] O. M. Ntwaeaborwa,[1] G. L. Fisher,[2] and J. J. Terblans[1]

[1]*Department of Physics, University of the Free State, P. O. Box 339, Bloemfontein, ZA9300, South Africa*
[2]*Physical Electronics USA, 18725 Lake Drive East, Chanhassen, Minnesota 55317, USA*
[3]*Tel: + 27514012926*
[*]*swarthc@ufs.ac.za*

Abstract: An Eu-doped $Sr_5(PO_4)_3F$ phosphor with a hexagonal apatite structure was prepared by a urea assisted combustion method. There was evidence of the reduction of Eu^{3+} to Eu^{2+} based upon the photoluminescence data. This was confirmed with X-ray photoelectron spectroscopy. Normally, it is very difficult to distinguish between two oxidation states with time-of-flight secondary ion mass spectrometry (TOF-SIMS), but it is shown that the parallel detection capability of the technique allows full molecular and isotopic characterization of the matrix chemistry. The two states were detected by the EuF^+ and EuF_2^+ species, ostensibly the Eu(II) and Eu(III) oxidation states, respectively.

OCIS codes: (250.5230) Photoluminescence; (300.2140) Emission; (300.6280) Spectroscopy, fluorescence and luminescence; (300.6490) Spectroscopy, surface; (300.6560) Spectroscopy, x-ray.

References and links

1. H. C. Swart, J. J. Terblans, O. M. Ntwaeaborwa, E. Coetsee, B. M. Mothudi, and M. S. Dhlamini, "Photon emission mechanisms of different phosphors," Nucl. Instrum. Meth. B **267**(16), 2630–2633 (2009).
2. P. Dorenbos, "Systematic behaviour in trivalent lanthanide charge transfer energies," J. Phys. Condens. Matter **15**(49), 8417–8434 (2003).
3. A. A. Kaminskii, "Laser crystals and ceramics: recent advances," Laser Photon. Rev. **1**(2), 93–177 (2007).
4. A. O. Wright, M. D. Seltzer, J. B. Gruber, and B. H. T. Chai, "Site-selective spectroscopy and determination of energy levels in Eu^{3+} doped strontium fluorophosphote," J. Appl. Phys. **78**(4), 2456–2467 (1995).
5. K. I. Schaffers, J. B. Tassano, A. B. Bayramian, and R. C. Morris, "Growth of Yb: S-FAP [Yb^{3+}:$Sr_5(PO_4)(3)F$] crystals for the Mercury laser," J. Cryst. Growth **253**(1-4), 297–306 (2003).
6. D. K. Sardar and F. Castano, "Characterization of spectroscopic and laser properties of Pr^{3+} in $Sr_5(PO_4)(3)F$ crystal," J. Appl. Phys. **91**(3), 911–915 (2002).
7. I. M. Nagpure, S. J. Dhoble, M. Mohapatra, V. Kumar, S. S. Pitale, O. M. Ntwaeaborwa, S. V. Godbole, and H. C. Swart, "Dependence of Eu^{3+} luminescence dynamics on the structure of the combustion synthesized $Sr_5(PO_4)_3F$ host," J. Alloy. Comp. **509**(5), 2544–2551 (2011).
8. I. M. Nagpure, S. S. Pitale, E. Coetsee, O. M. Ntwaeaborwa, J. J. Terblans, and H. C. Swart, "Lattice site dependent cathodoluminescence behaviour and surface chemical changes in $Sr5(PO_4)_3F$ host," Physica B: Condens. Matter **407**(10), 1505–1508 (2012).
9. A. Zounani, D. Zambon, and J. C. Cousseins, "Optical-properties of Eu^{3+} activated $Sr_{10}F_2(PO_4)_6$ elaborated by coprecipitation," J. Alloy. Comp. **188**(1–2), 82–86 (1992).
10. G. Särner, M. Richter, and M. Alden, "Investigations of blue emitting phosphors for thermometry," Meas. Sci. Technol. **19**(12), 125304 (2008).
11. C. Zhang, J. Yang, C. Lin, C. Li, and J. Lin, "Reduction of Eu^{3+} to Eu^{2+} in $MAl_2Si_2O_8$ (M = Ca, Sr, Ba) in air condition," J. Solid State Chem. **182**(7), 1673–1678 (2009).
12. S. J. Dhoble, I. M. Nagpure, N. S. Dhoble, and P. Molina, "Effect of Bi ion on $Eu^{2+} \leftrightarrow Eu^{3+}$ conversion in CaF_2:Eu phosphors for RPL dosimetry," J. Mater. Sci. **46**(22), 7253–7261 (2011).
13. G. J. Gao, S. Reibstein, M. Y. Peng, and L. Wondraczek, "Tunable dual-mode photoluminescence from nanocrystalline Eu-doped Li_2ZnSiO_4 glass ceramic phosphors," J. Mater. Chem. **21**(9), 3156–3161 (2011).
14. W. B. Im, J. H. Kang, D. C. Lee, S. Lee, D. Y. Jeon, Y. C. Kang, and K. Y. Jung, "Origin of PL intensity increase of $CaMgSi_2O_6$: Eu^{2+} phosphor after baking process for PDPs application," Solid State Commun. **133**(3), 197–201 (2005).
15. J. Zhang, M. Yang, H. Jin, X. Wang, X. Zhao, X. Liu, and L. Peng, "Self-assembly of $LaBO_3$:Eu twin microspheres synthesized by a facile hydrothermal process and their tunable luminescence properties," Mater. Res. Bull. **47**(2), 247–252 (2012).

#168333 - $15.00 USD Received 9 May 2012; revised 21 Jun 2012; accepted 4 Jul 2012; published 12 Jul 2012

16. P. Maślankiewicz, J. Szade, A. Winiarski, and Ph. Daniel, "Bridgman-Stockbarger growth and X-ray photoelectron spectroscopy study of $LiY_{1-x}Eu_xF_4$ crystals," Cryst. Res. Technol. **40**(4-5), 410–418 (2005).
17. A. Mezzi, S. Kaciulis, I. Cacciotti, A. Bianco, G. Gusmano, F. R. Lamastra, and M. E. Fragalà, "Structure and composition of electrospun titania nanofibres doped with Eu," Surf. Interface Anal. **42**(6-7), 572–575 (2010).
18. R. Vercaemst, D. Poelman, R. L. Van Meirhaeghe, L. Fiermans, W. H. Laflère, and F. Cardon, "An XPS study of the dopants' valence states and the composition of $CaS_{1-x}Se_x$:Eu and $SrS_{1-x}Se_x$:Ce thin film electroluminescent devices," J. Lumin. **63**(1–2), 19–30 (1995).

1. Introduction

Luminescent compounds and materials have numerous uses, most notably in detectors of various sorts, but also in consumer products such as displays, light emitting diode (LED) lighting and watches. The device, or application, in which a luminescent material is used, depends largely on its emission properties including color, brightness and decay rate. The emission properties, whether of a fast decay rate fluorescent material or a slow decay rate phosphorescent material, are defined by the chemical composition and the physical structure of the luminescent material [1]. The brightness and the decay rate can be affected significantly by trace contaminants, or toxins. Spectroscopic properties of trivalent rare-earths (RE) (such as Pr^{3+}, Nd^{3+}, Ho^{3+}, Er^{3+} and Tm^{3+}) incorporated into crystals of strontium fluorapatite (SFAP), or $Sr_5(PO_4)_3F$, have been reported previously [2–6]. In this paper, we have used a *nanoTOF* time-of-flight secondary ion mass spectrometry (TOF-SIMS) instrument to visualize the trace-level chemical inhomogeneities in a Eu-doped phosphor powder. The Eu dopant is present in the + 3 oxidation state, or Eu(III), throughout the phosphor. However, the phosphor is believed to be contaminated with small quantities of the + 2 oxidation state, or Eu(II). An important characteristic of TOF-SIMS is the ability to visualize chemical information in a spatially resolved manner. TOF-SIMS also combines parallel detection so that the entire mass spectrum is available for chemical identification with high sensitivity so that trace-level chemistries may be identified. The *nanoTOF* SIMS is equipped for chemical imaging of topographically rough surfaces.

2. Experimental setup

$Sr_5(PO_4)_3F:Eu^{3+}$ phosphors were prepared via the combustion assisted method using urea as fuel and heating at 500-600 °C. All the chemicals used in the phosphor preparation were of GR grade with 99.99% purity. The starting materials were strontium nitrate ($Sr(NO_3)_2 \cdot 4H_2O$), di-ammonium hydrogen phosphate ($NH_4H_2(PO_4)$), ammonium fluoride (NH_4F) and Eu nitrate ($Eu(NO_3)_3 \cdot 6H_2O$). All the reagents in the required amounts were dissolved in appropriate solvent and mixed together to obtain a homogeneous solution. Urea (NH_2CONH_2) was dissolved in water. The urea solution was added to the metal nitrate solutions with vigorous stirring. After stirring for about 30 min., a semi-solid mass was obtained. This mass was transferred to a muffle furnace preheated to 500-600 °C and after 5 min. a porous product was obtained which was designated as the as-prepared sample. X-ray diffraction (XRD) data (not shown) [7] indicated that the major crystalline phases from the as-prepared powder samples were identical to the hexagonal apatite structure of $Sr_5(PO_4)_3F$ as referenced in JPCDS file No. 017-0609. The photoluminescence (PL) lifetime decay and time-resolved data of the phosphors were recorded using a CD-920 unit from Edinburgh Analytical Instruments, UK. The system is equipped with a variable temperature liquid nitrogen cryostat OptistatDN (Oxford) which enabled studies on temperature related changes in the emission spectra in the 77–300K temperature range. The reciprocal linear dispersion for both the monochromators associated with the spectrometer is 1.8 nm/mm. The luminescence spectra for the sample were recorded at room temperature. Suitable filters were interposed between the sample and the fluorescence monochromator to prevent the recording of the second order exciting radiation. Initially, fluorescence decay measurements were carried out at different time to amplitude converter (TAC) settings in the range of 50 ns–40 ms using the Edinburgh CD-920 spectrometer. The specified range for decay time measurements was extended to include the long-lived component of the emission. On the basis of these studies, subsequent measurements, for obtaining excitation and emission spectra were carried out using two

#168333 - $15.00 USD Received 9 May 2012; revised 21 Jun 2012; accepted 4 Jul 2012; published 12 Jul 2012

different settings viz. (A) With the Xenon flash lamp repetition rate of 40 kHz and a TAC range of 0–5 μs and (B) With the Xenon flash lamp repetition rate of 0.5 kHz and a TAC range of 0–40 ms. The measurements under these conditions enabled the recording of both fast decay (ns) and slow decay (ms and longer) components of the emission spectrum of the sample. For obtaining emission/excitation spectra, fluorescence decay measurements were carried out at discrete wavelength positions in the wavelength range of interest and the data was stored in different data files. Subsequently, software associated with time-resolved spectral analysis, allowed processing of these data files to produce a plot of spectral intensity measurement versus wavelength. For recording of excitation and fluorescence spectra, slit-widths for the respective monochromators were varied between 0.5 and 2.5 mm which corresponded to bandwidth of 1–5 nm. The fluorescence spectra were recorded over the spectral range of 200–750 nm. The X-ray photoelectron spectroscopy (XPS) measurements were carried out on a PHI 5000 *VersaProbe* spectrometer using a monochromatic Al K_α radiation source ($h\nu$ = 1253.6 eV). For high resolution spectra, the hemispherical analyzer pass energy was maintained at 11.3 eV. Measurements were performed using either a 1 eV/step and 45 min. acquisition time (binding energies ranging from 0 to 1400 eV) for survey scans, or a 0.1 eV/step and 20-30 min. acquisition time for the high resolution scans. The sample area analyzed was less than 1 mm^2 and the pressure during acquisition was typically under 1×10^{-8} Torr. For TOF-SIMS measurements, the phosphor powder was used in the as-prepared state and was mounted onto a silicon substrate using double-sided hydrocarbon tape. All the TOF-SIMS measurements were performed on a PHI TRIFT V *nanoTOF*. A pulsed 30 keV Au^+ primary ion beam, operated at a DC current of 100 pA, was used to acquire chemical images of the phosphor in both the positive and the negative secondary ion polarities. The analytical field-of-view was 200 μm x 200 μm with a 256 pixel x 256 pixel digital raster, and the primary ion dose was maintained well within the static limit, i.e. ≤ $1.2x10^{11}$ Au^+/cm^2, for each analysis. Charge compensation was achieved with a dual-beam (≤ 15 eV e^- and ≤ 10 eV Ar^+) charge neutralizer. A raw data stream file was collected to allow full post-acquisition evaluation (i.e. retrospective analysis) of the data.

3. Results

Photoluminescence analysis and decay study

Figure 1 illustrates the photoluminescent emission spectra of the $Sr_5(PO_4)_3F:Eu_{1m\%}$ phosphor (NB 1m% = 1 mol%). The spectra are from previous obtained results from Nagpure et al. [7,8]. The excitation spectra monitored at an emission of 616 nm is shown as an inset. A similar excitation spectrum (not shown) with less intensity was obtained for the 440 nm emission peak. The PL emission spectrum was recorded when monitoring the charge transfer excitation band centered at 243 nm. The PL emission spectrum shows weak blue broad band emission in the region of 430-450 nm that is due to the $4f^6 5d \rightarrow 4f^7$ transitions of the Eu^{2+} state. A much better resolved Eu^{2+} peak was obtained with CL spectroscopy [8]. The emission peaks due to $^5D_0 \rightarrow {}^7F_1$, $^7F_2$ and $^7F_3$ transitions are observed at 593, 616 and 653 nm, while the emissions observed at 680 and 705 nm are due to the $^5D_0 \rightarrow {}^7F_j$ transitions of Eu^{3+} state [9]. The decay study was carried out by monitoring emissions at 440 and 616 nm separately to determine the lifetime and valency of the dopant ion. The decay data of the 440 nm emission from Eu^{2+} were fitted with a single exponential equation and a decay time (ζ) of 500 ns was obtained as shown in the inset of Fig. 1. This corresponds to the decay time of the same emission reported by Sarner and associates [10]. On the other hand, the decay data of the 616 nm emission from Eu^{3+} were fitted with a double exponential equation. The decay times of ζ_1 = 1.5 ms and ζ_2 = 3.9 ms were obtained and are also shown in the inset of Fig. 1. They are consistent with the decay times of Eu^{3+} ions reported by Zhang and associates [11]. The PL emission and decay data confirm the presence of both Eu^{2+} and Eu^{3+} ions in the $Sr_5(PO_4)_3F:Eu_{1m\%}$ phosphor. The appearance of the weak blue emission and prominent red emission from the $Sr_5(PO_4)_3F:Eu_{1m\%}$ phosphor, and the distribution and lattice site occupancy of Eu^{2+} and Eu^{3+} dopants, were discussed in detail by Nagpure and associates [7,8]. UV

#168333 - $15.00 USD Received 9 May 2012; revised 21 Jun 2012; accepted 4 Jul 2012; published 12 Jul 2012

photo-excited Eu^{2+} and Eu^{3+} luminescence from CaF_2:Eu phosphors were investigated by Dhoble et al. [12]. From their data the Eu^{2+} broadness of the emission peak was in the order of 25 nm. For further confirmation of the 440 nm as a Eu^{2+} emission peak, the PL emission spectra of the Eu ion doped $Sr_5(PO_4)_3F$ samples as a function of annealing temperature [7] were obtained. The sample was annealed in air atmosphere. It is clear from the spectra that with an increase in the annealing temperature, there was a reduction in the fluorescence intensity of the Eu signal along with the evolution of a weak signal at ≈430–450 nm. With the increase in annealing temperature, the PL due to the Eu^{3+} intensity decreased and the PL from the Eu^{2+} intensity increased suggesting a reduction of Eu^{3+} to Eu^{2+} in the system.

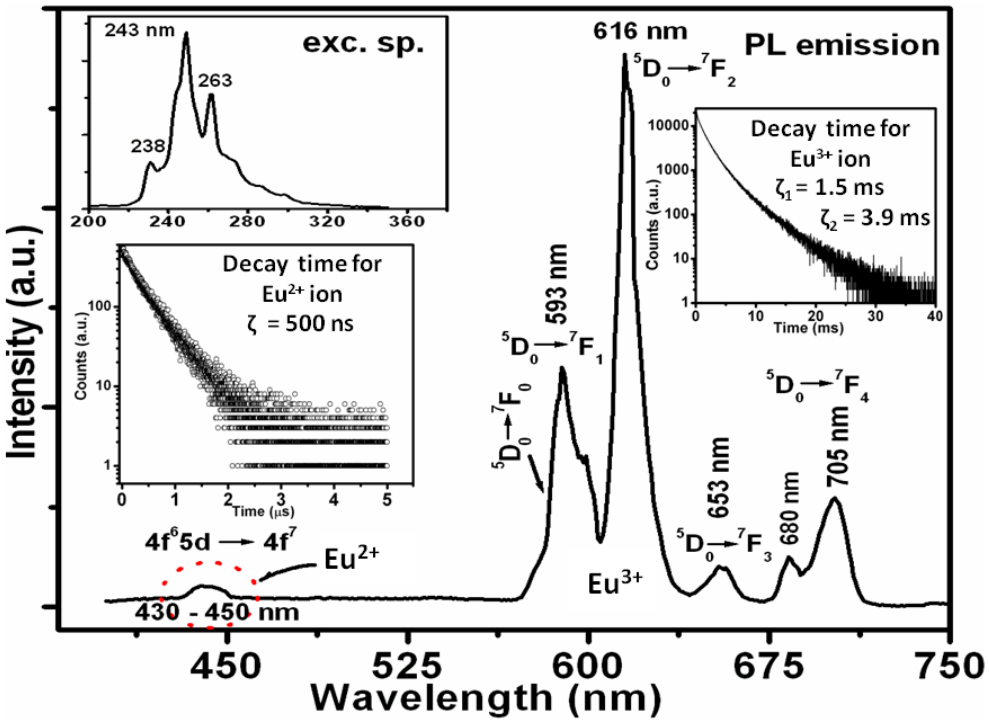

Fig. 1. The emission spectrum of the $Sr_5(PO_4)_3F:Eu_{1m\%}$ phosphor excited at 242 nm. The excitation spectrum monitored at 616 nm is shown as an inset. The decay curves of the Eu^{2+} and Eu^{3+} are also shown as insets [7,8].

Oxidation state of Eu ion dopant with XPS analysis

While the emission from Eu^{3+} is characterized by narrow emission bands mainly in the red part of the spectrum, the emission of Eu^{2+} can be changed over the entire visible spectrum by appropriate choice of the host compound. In halophosphate hosts, the Eu^{2+} emission is generally situated in the blue part of the spectrum [13]. In this work, the valence and oxidation states of Eu ions in the as-synthesized $Sr_5(PO_4)_3F:Eu_{1m\%}$ phosphor were determined by the XPS technique. The XPS spectra of the Eu-3d core level of the $Sr_5(PO_4)_3F:Eu_{1m\%}$ samples are shown in Fig. 2. The two peaks at 1134.3 and 1124.1 eV can be attributed to Eu^{3+} and Eu^{2+} $3d_{5/2}$ core levels, respectively [14,15] while the other two peaks at 1165.2 and 1153.9 eV, can be attributed to Eu^{3+} and Eu^{2+} $3d_{3/2}$ core levels, respectively [16]. The shake-up satellite peaks due to the chemical shift between the Eu^{2+} and Eu^{3+} oxidation states [16,17] were also observed. The shake-up satellite peaks at 1138.1 and 1128.3 eV can respectively be attributed to the Eu^{3+} and Eu^{2+} $3d_{5/2}$ core levels, while those at 1168.7 and 1157.2 eV can respectively be attributed to Eu^{3+} and Eu^{2+} $3d_{3/2}$ core levels. The peak position and binding energy from the XPS analysis, corresponding to the $3d_{5/2}$ and $3d_{3/2}$ core levels of the Eu ion,

#168333 - $15.00 USD Received 9 May 2012; revised 21 Jun 2012; accepted 4 Jul 2012; published 12 Jul 2012

suggesting that Eu is present in both the Eu^{2+} and Eu^{3+} oxidation states. The XPS analysis also indicates that the ratio of Eu^{2+}:Eu^{3+} is 40:60%. It must be pointed out that Vercaemst et al. [18] have found that XPS measurements on Eu doped $CaS_{1-x}Se_x$ thin films reveal that Eu^{2+} is readily oxidized during XPS measurements and concluded that extensive XPS measurements resulted in a Eu^{3+} state.

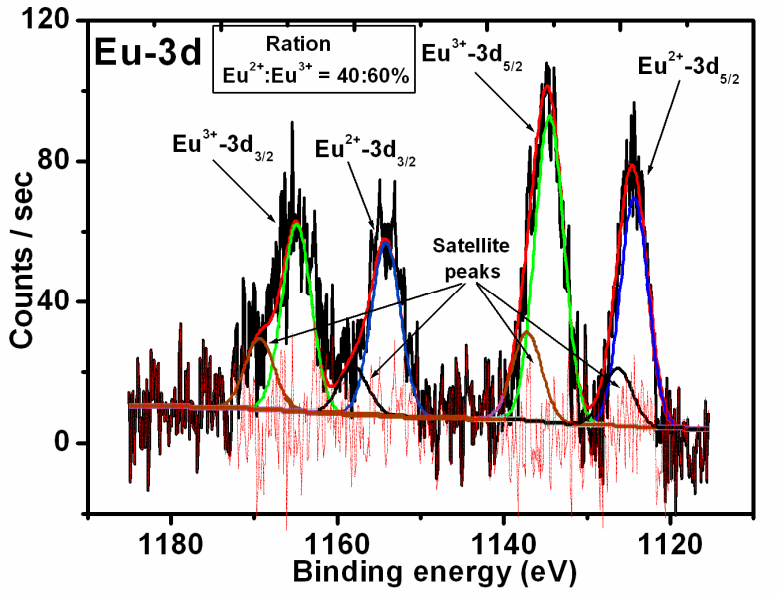

Fig. 2. The Eu 3d high resolution XPS spectrum of the $Sr_5(PO_4)_3F:Eu_{1m\%}$ phosphor.

Oxidation states of Eu ion dopant with TOF SIMS analysis

The optical and the corresponding TOF-SIMS total ion image of a 200 µm x 200 µm field-of-view of the phosphor powder are shown in Fig. 3(A) and 3(B). These images reveal the severe topography of the powder which has particle sizes ranging from approximately 20 µm to approximately 100 µm in diameter. The SIMS mass spectrometer allows efficient and uniform collection of secondary ion signals from all parts of the particles for full chemical characterization. The $Sr_2PO_4^+$ (271m/z) ion image is shown in Fig. 3(C). It is clear that the material is uniformly spread out across the phosphor particles. Similar ion images of PO_3^- and PO_4^- also showed the uniformness thereof across the phosphor particles. Several elemental and chemical images of the phosphor particles are shown in Fig. 4. The hydrocarbon mounting tape is observed in Fig. 4(A). Some hydrocarbon signal is observed across the surface of the phosphor particles which ostensibly arises from contamination produced during the process of sample mounting. The phosphor is strontium-based as the image in Fig. 4(B) illustrates, wherein each particle is clearly observed. The phosphor is doped with Eu in the + 3 oxidation state, Eu(III), which is clearly observed as EuF_2^+ in Fig. 4(D) to be homogeneously distributed throughout the particles as a fluorine complex. Note that fluorine is a known constituent of the phosphor composition. Based on the PL emission and XPS characterization of the phosphor, it is reasonable to speculate that some of the Eu dopant had been reduced to the + 2 oxidation state, Eu(II). The image of EuF^+ in Fig. 4(C) reveals a distribution of Eu(II) that is highly inhomogeneous and distinct from that of the Eu(III) dopant. The differences in spatial distribution of EuF^+ and EuF_2^+ indicates that the appearance of these species is not related to simple ion fragmentation (i.e. a "SIMS effect"), nor can it be explained by a difference in fluorine distribution since the fluorine signal is homogeneous. Rather, it is likely that these components arise clearly from a difference in the oxidation state of the Eu. Figure 5 shows the false colour overlay images of the different elements. The distribution of the

#168333 - $15.00 USD Received 9 May 2012; revised 21 Jun 2012; accepted 4 Jul 2012; published 12 Jul 2012

different oxidation states is quite clear from these images; the Eu(III) dopant is much more homogeneously distributed while the Eu(II) contaminant is more concentrated at certain points. As pointed out by Nagpure et al. [7] there are two Sr sites on which Eu ions can be substituted in this phosphor. One site is coordinated by oxygen atoms only, while the other site contains both F and O ions in the first coordination sphere and it must therefore be mentioned that this may have an implication on the valence mapping of the EuF^{+} and EuF^{2+} alone.

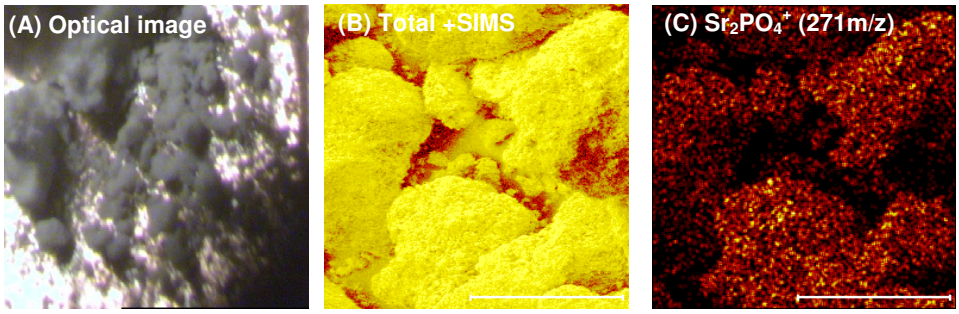

Fig. 3. Images of the Eu-doped phosphor powder. (A) Optical image at the analysis position. The powder particles range in size from ~20 µm to ~100 µm. (B) Total ion image (+ SIMS) of the phosphor particles within a 200 µm x 200 µm field-of-view. The marker is 100 µm. (C) Image of the $Sr_2PO_4^+$ (271m/z) ion signal.

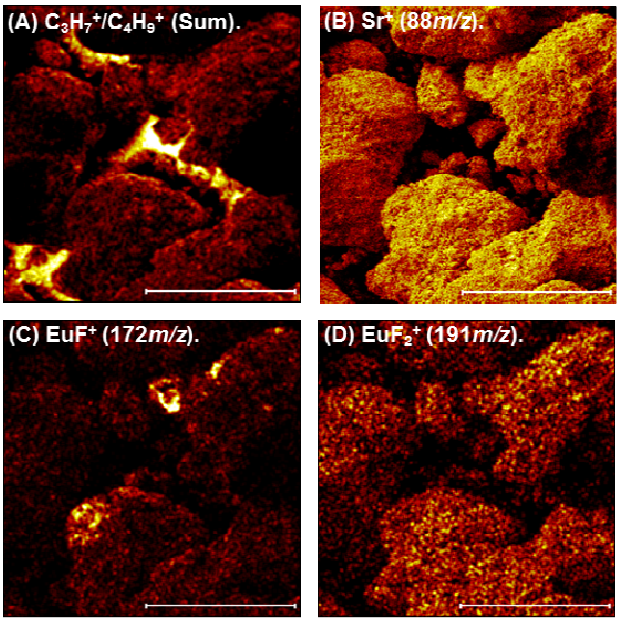

Fig. 4. TOF-SIMS chemical images of the Eu-doped phosphor powder. Each image was collected in the positive secondary ion polarity (+ SIMS) and shows specific elemental or chemical distributions across the surface of the particles observed within a 200 µm x 200 µm field-of-view (the marker is 100 µm). (A) Image of the summed $C_3H_7^+$ (43 m/z) and $C_4H_9^+$ (57 m/z) ion signals. (B) Image of the Sr^+ (88 m/z) ion signal. (C) Image of the EuF^+ (172 m/z) ion signal. (D) Image of the EuF_2^+ (191 m/z) ion signal. The organic fragments shown in panel A arise from the mounting tape and are observed to have contaminated the powder surface during mounting.

#168333 - $15.00 USD Received 9 May 2012; revised 21 Jun 2012; accepted 4 Jul 2012; published 12 Jul 2012

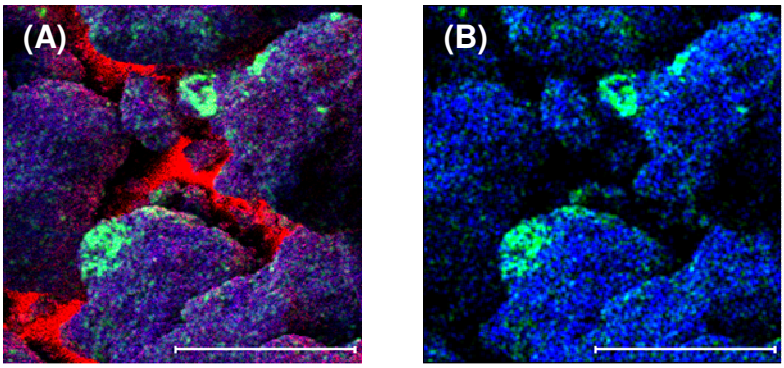

Fig. 5. (A) False colour overlay of the $C_3H_7^+/C_4H_9^+$ organic fragment ions (image sum; red), the $Eu(II)F^+$ (172 m/z; green) poison ion, and the $Eu(III)F_2^+$ (191 m/z; blue) dopant ion. ((B) False colour overlay of the $Eu(II)F^+$ (172 m/z; green) poison ion and the $Eu(III)F_2^+$ (191 m/z; blue) dopant ion. In each image, the field-of-view is 200 µm x 200 µm and the marker is 100 µm. Note that while the Eu(II) poison is distributed throughout the phosphor particles, the localization observed within certain particles improves the confidence regarding the identification of a distinct Eu oxidation state in the absence of pure reference materials.

4. Conclusion

Both PL and XPS indicate that both Eu^{2+} and Eu^{3+} oxidation states exist in the as-prepared $Sr_5(PO_4)_3F:Eu_{1m\%}$ phosphor. The results also show that the Eu^{2+} quantity is also much more than just the original amount of the expected contaminant. TOF-SIMS chemical imaging was conducted on the Eu-doped phosphor to observe the differences in oxidation state and distribution of the Eu(III) dopant and the Eu(II) poison. The high sensitivity of TOF-SIMS enables detection of species having a low abundance, and the parallel detection capability allows full molecular and isotopic characterization of the matrix chemistry. It was possible to efficient and uniformly collected secondary ions from all parts of the topographically rough samples without image artifacts.

Acknowledgments

The authors are thankful to the University of the Free State (UFS) and the South African National Research Foundation (NRF) for the financial support, and to Physical Electronics USA for the TOF-SIMS measurements.

#168333 - $15.00 USD Received 9 May 2012; revised 21 Jun 2012; accepted 4 Jul 2012; published 12 Jul 2012